International Journal of Nanomedicine

Dovepress
open access to scientific and medical research

Open Access Full Text Article

ORIGINAL RESEARCH

Comparison of the Therapeutic Effect of Allogeneic and Xenogeneic Small Extracellular Vesicles in Soft Tissue Repair

This article was published in the following Dove Press journal:
International Journal of Nanomedicine

Jia Dong[1–3,*]
Yue Wu[1,2,4,*]
Yan Zhang[1–3]
Mei Yu[1,2]
Weidong Tian[1–3]

[1]State Key Laboratory of Oral Disease, Engineering Research Center of Oral Translational Medicine, Ministry of Education, West China School of Stomatology, Sichuan University, Chengdu, Sichuan, People's Republic of China; [2]National Engineering Laboratory for Oral Regenerative Medicine, Sichuan University, Chengdu, Sichuan, People's Republic of China; [3]Department of Oral and Maxillofacial Surgery, West China Hospital of Stomatology, Sichuan University, Chengdu, Sichuan, People's Republic of China; [4]Department of Oral & Maxillofacial Surgery, Xiangya Stomatological Hospital & School of Stomatology, Central South University, Changsha, Hunan, People's Republic of China

*These authors contributed equally to this work

Purpose: Small extracellular vesicles (sEV) are a heterogeneous group of vesicles that consist of proteins, lipids and miRNA molecules derived from the cell of origin. Although xenogeneic sEV have been applied for soft tissue regeneration successfully, the regeneration effect of allogeneic and xenogeneic sEV has not been compared systematically.

Methods: Our previous study has shown that sEV derived from rat adipose tissue successfully induced neoadipose regeneration. In this study, sEV were isolated from rat adipose tissue (r-sEV-AT) and porcine adipose tissue (p-sEV-AT), the morphology, size distribution and marker proteins expression of r-sEV-AT and p-sEV-AT were characterized. Besides, the sEV/AT ratio was evaluated and compared between r-sEV-AT and p-sEV-AT. Rat adipose-derived stromal/stem cells (rASCs) and rat aorta endothelial cells (rECs) were adopted to test the cellular response to allogeneic and xenogeneic sEV-AT. The effects of allogeneic and xenogeneic sEV-AT on host cells migration and neoadipose formation were evaluated in a subcutaneous custom-designed model. A full-thickness skin wound healing model was used to further compare the ability of allogeneic and xenogeneic sEV-AT in inducing complex soft tissue regeneration.

Results: p-sEV-AT showed similar morphology and size distribution to r-sEV-AT. Marker proteins of sEV were detected in both r-sEV-AT and p-sEV-AT. The sEV/AT ratio of porcine was slightly higher than that of rat. The effects of r-sEV-AT and p-sEV-AT on the differentiation of rASCs and rECs showed no significant difference. When allogeneic and xenogeneic sEV-AT were subcutaneously implanted into the back of SD rats, the host cells chemotactic infiltration was observed in 1 week and neoadipose tissue formation was induced in 8 weeks; no significant difference was observed between allogeneic and xenogeneic sEV-AT. For complex soft tissue regeneration, both allogeneic and xenogeneic sEV-AT significantly promoted wound re-epithelialization, granulation tissue formation and hair follicle regeneration and then accelerated skin wound healing.

Conclusion: Our results demonstrated that sEV derived from the same tissues of different species might be loaded with similar therapeutic substance benefitting tissue repair and regeneration, and paved the way for future research aimed at xenogeneic sEV application.

Keywords: xenogeneic, small extracellular vesicles, neoadipose formation, skin wound repair

Correspondence: Mei Yu; Weidong Tian
State Key Laboratory of Oral Disease, West China School of Stomatology, Sichuan University, No. 14, 3rd Sec., Ren Min Nan Road, Chengdu, Sichuan Province 610041, People's Republic of China
Tel/Fax+86-28-85503499
Email yumei925@hotmail.com; drtwd@sina.com

Introduction

Small extracellular vesicles (sEV) are a heterogeneous group of cells-derived membrane vesicles that consist of proteins, lipids, and coding or noncoding RNA molecules derived from the cells of origin.[1,2] A lot of studies have shown that many proteins[3–5] and microRNAs[6–9] are species-specific. Even for some conserved

miRNAs, their targeting in different species will be different, like let-7 miRNA family.[10–13] The molecules-loaded vesicles, in physiological or pathological conditions, are involved in the regulation and maintenance of reproduction, blood coagulation, cell death, stem cell expansion, neuronal communication, tumorigenesis, tissue repair and inflammation, among others.[14–18] For example, in the treatment of myocardial infarction (MI), Tseliou et al[19] found that the ejection fraction increased by 15% after injection of sEV secreted by rat cardiosphere-derived cells into a rat myocardial infarction model. Ibrahim et al[20] and Gallet et al[21] injected sEV secreted by human cardiosphere-derived cells to mice or mini-pig model, respectively, and both of the results showed that xenogeneic sEV was effective in the repairing of myocardial infarction and the ejection fraction increased 10%. Both allogeneic and xenogeneic sEV had shown a constructive and positive impact on soft tissue repair. By comparing these studies, we could find that the application of allogeneic sEV could increase the ejection fraction by 15%, while the application of xenogeneic sEV could only increase the ejection fraction by 10%. Although we suspected that species might have an impact on the outcome of the treatment, in these studies, the differences in the sEV isolation method, route of administration, and animal model might lead to the differences in repairing of myocardial infarction. Therefore, the direct correlation between the efficacy of tissue repair and species of sEV was still unknown.

Adipose tissue was initially regarded as a type of tissue storing excess nutrients. However, recent studies demonstrated that adipose tissue could function as an endocrine organ that produced and secreted a wide range of mediators regulating adipose tissue and important distant targets (such as the liver, skeletal muscle, the pancreas and the cardiovascular system).[22] In addition to adipocytes, the other cell types such as precursor, endothelial, immune cells and fibroblasts in the adipose tissue could also contribute to the release of sEV to mediate the cross-talk between adipose tissue and other distal tissues.[23,24] Our previous study has shown sEV derived from adipose tissue (sEV-AT) could trigger adipogenic signaling in ASCs, resulting in adipogenic differentiation,[25] so we chose sEV-AT as the representative sEV to compare the potential of allogeneic and xenogeneic sEV in regenerative medicine.

There is an emerging need for soft-tissue replacements in the field of reconstructive surgery for the treatment of congenital deformities, posttraumatic repair and cancer rehabilitation. The stem cell-based therapy or acellular approaches to generate engineering adipose tissue were studied to develop an ideal soft tissue replacement which is well-vascularized, maximum neotissue formation and long-term volume maintenance. We have successfully induced neoadipose tissue regeneration with sEV-AT in a subcutaneous silicone tube model.[26] In this study, we chose the same model to compare the effectiveness of allogeneic and xenogeneic sEV-AT in inducing neoadipose tissue formation. In order to further compare the repair ability of sEV-AT in more complex soft tissue regeneration, a well-established full-thickness skin wound healing model was used.

Materials and Methods

Animals

Animals were obtained from Dashuo Experimental Animal Co. Ltd. (Chengdu, China). This study was reviewed and approved by the Ethics Committees of the State Key Laboratory of Oral Diseases, West China School of Stomatology, Sichuan University. The approval number is WCHSIRB-D-2019-032. The care and use of the laboratory animals followed the guidelines of the Institutional Animal Care and Use Committee of West China School of Stomatology, Sichuan University.

Preparation of sEV-AT

Our previous studies demonstrated that sEV could be successfully isolated from rat adipose tissue using a kit-based ultrafiltration method.[26] Therefore, we chose the same method with the following modifications to isolate r-sEV-AT and p-sEV-AT from rat and porcine adipose tissue, respectively. Fat pads were minced into small pieces and transferred into a Celstir spinner flask (Wheaton). Serum-free α-modified Eagle's medium (α-MEM, HyClone) with 100 U/mL penicillin and 100 U/mL streptomycin was added into the flask and the tissues were cultured in a 5% CO_2-95% air atmospheric condition at 37°C with speed at 100 rpm for 2 days. Tissue pieces were removed by gauze and the debris of tissues and cells were removed by centrifugation at 2000 rpm for 20 min, followed by a 40 μm filter (BD falcon). The supernatant obtained at this time was called adipose tissue extract (ATE). For further isolation of sEV-AT, ATE was filtered through 0.22 μm filters (Millipore), then concentrated by Ultracel-3 membrane (Millipore) at 5000 g, 4°C for 30

min, further filtrated by Ultracel-100 membrane (Millipore) at 5000 g, 4°C for 30 min. The concentrated ATE was mixed with the Total Exosome Isolation™ reagent (Life Technologies) at 4°C overnight and spun down at 10,000 g, 4°C for 1 h to obtain sEV-AT.

Characterization of sEV-AT

sEV-AT was resuspended in PBS and the concentration of sEV-AT was measured in terms of their protein content determined by the bicinchoninic protein assay method using the manufacturer's protocol (BCA Protein Assay Kit, KeyGEN BioTECH). The morphology of sEV-AT was observed by Transmission Electron Microscopy (TEM). The particle size and size distribution of sEV-AT were determined by ZetasizerNano ZS analysis system (Zetasizer version 6.12, Malvern Instruments, UK). Details were described in our previous studies.[25,26] The expression of actin, CD63, TSG101 and CD9 in sEV-AT was detected by Western blot.

Western Blot

Thirty-microgram sEV-AT was dissolved in RIPA Lysis Buffer (KeyGEN, China), resolved on a 10% polyacrylamide gel, and blotted on to a nitrocellulose membrane. The membranes were blocked and then incubated with primary antibodies against CD9 (Zen Bioscience, 220,642), TSG101 (Zen Bioscience, 512,216), CD63 (Zen Bioscience, 510,953) and actin (Abcam, ab3280) at 4°C overnight, followed by horseradish peroxidase (HRP)-conjugated secondary antibodies for 1 h at room temperature. Immobilon Western Chemiluminescent HRP Substrate (Millipore) was used for the detection following the manufacturer's instructions. Signals were visualized with a ImageQuant LAS 4000 mini machine (GE Healthcare).

Cells Isolation and Culture

Adipose-derived stromal/stem cells (ASCs) were isolated from SD rats. Inguinal fat pads were collected, cut into small pieces, and digested with 0.075% type I collagenase for 30 min at 37°C. The mixture was washed with PBS and centrifuged at 1000 rpm for 5 min, and the remaining pellet was cultured in α-modified Eagle's medium (α-MEM; HyClone), 10% fetal bovine serum (FBS; Gibco), 100 U/mL penicillin, and 100 U/mL streptomycin. Cells were cultured in a 5% CO_2-95% air atmospheric condition at 37°C. The medium was replaced every 2 days, and cell passaging was performed when the monolayer of adherent cells reached 90% confluence.

Aorta endothelial cells (ECs) were obtained from the thoracic aorta of SD rats as described by Tian et al[27] and were cultured in endothelial cells growth medium (EGM-2MV; Lonza). Cultures were maintained in a 5% CO_2-95% air atmospheric condition at 37°C. The medium was replaced every 2 days, and cell passaging was performed when the monolayer of adherent cells reached 90% confluence.

sEV-AT Labeling and Cellular Uptake

Hundred-microgram r-sEV-AT and p-sEV-AT were labeled with 1μg membrane-labeling dye DiO (Invitrogen) in serum-free α-MEM at 37°C for 20 min according to the manufacturer's protocol, then DiO-labeled sEV-AT was re-purified with the Total Exosome Isolation™ reagent (Life Technologies) to remove the unincorporated dye. The obtained DiO-labeled sEV-AT pellet was resuspended in serum-free α-MEM. Next, rASCs were co-cultured with DiO-labeled sEV-AT for 6 h, washed with PBS, fixed in 4% paraformaldehyde, stained with phalloidin (Invitrogen) and DAPI, washed with PBS and imaged by confocal microscopy (Olympus FV1000, Japan).

Cell Differentiation Induced by sEV-AT

rADSCs or rECs, $1X10^5$ cells per well in 12-well plates, were continuously co-cultured with 50 μg/mL r-sEV-AT or p-sEV-AT (50 μg sEV-AT in 1 mL culture medium) and the culture medium containing sEV-AT was changed every 2 days to maintain the treatment effect. The cells cultured with the basal medium alone were used as negative control. After co-culturing rECs with sEV-AT for 4 days, the relative expressions of angiogenic genes (*CD31*, *VEGF*, *FGF2* and *angiogenin*) were determined by real-time PCR. Similarly, the relative expressions of adipogenic genes (*PPARγ*, *C/EBPα*, *adiponectin* and *FABP4*) in rASCs were analyzed by real-time PCR after 5 days and 10 days of induction.

Tube Formation Assays

rECs ($1.5X10^4$), suspended in endothelial cells growth medium (EGM-2MV, Lonza) with 50 μg/mL r-sEV-AT or p-EV-AT (10 μg sEV-AT in 200 μL culture medium) respectively, were seeded onto 96-well plates coated with Matrigel (Corning). After incubation for 5 h, phase-contrast images were acquired on an inverted microscope (Olympus). The total number and length of all tubing

within each field were measured using Image Pro-Plus software.

qRT-PCR

The RNAiso Plus (TaKaRa Biotechnology, Japan) was used to extract total RNA, which was reverse transcribed into cDNAs using the RevertAid First Strand cDNA Synthesis Kit (Thermo Scientific). The synthesized cDNAs were amplified with SYBR Premix ExTaq (TaKaRa Biotechnology, Japan) using QuantStudio 6 Flex Real-Time PCR System (Life Technologies, Carlsbad, CA). The PCR cycling parameters were 95°C for 2 min, 44 cycles of 95°C for 5 s, and 60°C for 30 s. The results were analyzed using the $2^{-\Delta\Delta CT}$ method and normalized to the reference GAPDH gene. This experiment was repeated at least three times. Primer sequences were listed in Supplementary Table S1.

In vivo Experiments

In the adipose tissue regeneration model, 60 μL Matrigel (Corning) was mixed with 60 μL PBS contained 360 μg r-sEV-AT or p-sEV-AT. The final concentration of sEV-AT of these mixtures was 3 mg/mL. Sixtymicroliter Matrigel (Corning) mixed with 60 μL PBS was adopted as the blank group. Then, we transferred them into a custom-designed silicone tube to maintain the integrity and shape of implant material, and subcutaneously implanted into the back of SD rats. The incision was closed with 3/0 nylon suture. All rats were sacrificed via the Ethics Committees approved methods at 3D, 5D, 1W, 2W, 4W and 8W for analysis of the implants.

In the skin wound healing model, full-thickness excisional skin wounds (15 mm in diameter) were made on the back of SD rats. A custom-designed silicone device was used to keep the wound area clean, free of debris and stabilized and prevent wound contraction. Hundred-microliter Polyvinyl Alcohol (PVA) was mixed with 100 μL PBS contained 600 μg r-sEV-AT or p-sEV-AT. The final concentrations of sEV-AT of these mixtures were 3 mg/mL. Hundred-microliter PVA was mixed with 100 μL PBS was as the blank group. Then, the mixtures were dropped onto the surface of the wound. In order to ensure the therapeutic effect of sEV-AT, the wounds were treated once a week. Digital photographs were taken at 0D, 7D, 10D, 14D, and 21D, and the wound area was measured using the Image J software. Treated rats were sacrificed at 10D and 21D, respectively, via the Ethics Committees approved methods and samples were harvested for further testing.

Hematoxylin and Eosin (H&E) Staining

The samples were harvested and fixed in 4% neutral paraformaldehyde overnight. After removing the tubes, remained tissues were dehydrated using graded ethanol and paraffin-embedded and sectioned into 5 μm thick sections for H&E staining and immunochemical staining.

Immunochemical Staining

Sections were blocked for 2 h and then incubated overnight at 4°C with primary antibodies. Primary antibodies against and perilipin A (Abcam, ab3526) were used in this study to analyze adipocytes. The secondary antibody was shown by the DAB kit (Gene Tech, Shanghai, China).

Statistical Analysis

Results are expressed as mean value–standard deviation. One-way ANOVA with Tukey posthoc test was used to determine the level of significance. A value of $p < 0.05$ was considered statistically significant.

Results

Characterization of r-sEV-AT and p-sEV-AT

Our previous studies demonstrated that sEV could be successfully isolated from rat adipose tissue using a kit-based ultrafiltration method and possessed the defining characteristics of sEV.[25,26] In this study, we used the same method to isolate adipose tissue-derived sEV from rat and porcine. Firstly, the general characteristics of adipose tissue from rat and porcine were compared. The color of native adipose tissue from both rat and porcine showed to be white and the adipose tissue of rat appeared soft, but that of pig appeared dense. H&E staining revealed that the adipocytes of porcine were larger than that of rat. The diameter of adipocytes of rat was less than 50 μm, but the diameter of adipocytes of porcine could reach 100 μm (Figure 1A). Although the size of adipocytes observed in two species was different, the shape and size distribution of r-sEV-AT and p-sEV-AT showed to be similar. Transmission electron microscopy (TEM) analysis confirmed that the presence of round shaped vesicles surrounded by a bilayer membrane in each sample (Figure 1B). NanoSight analysis indicated that the diameter of r-sEV-AT and p-sEV-AT both ranged from 80

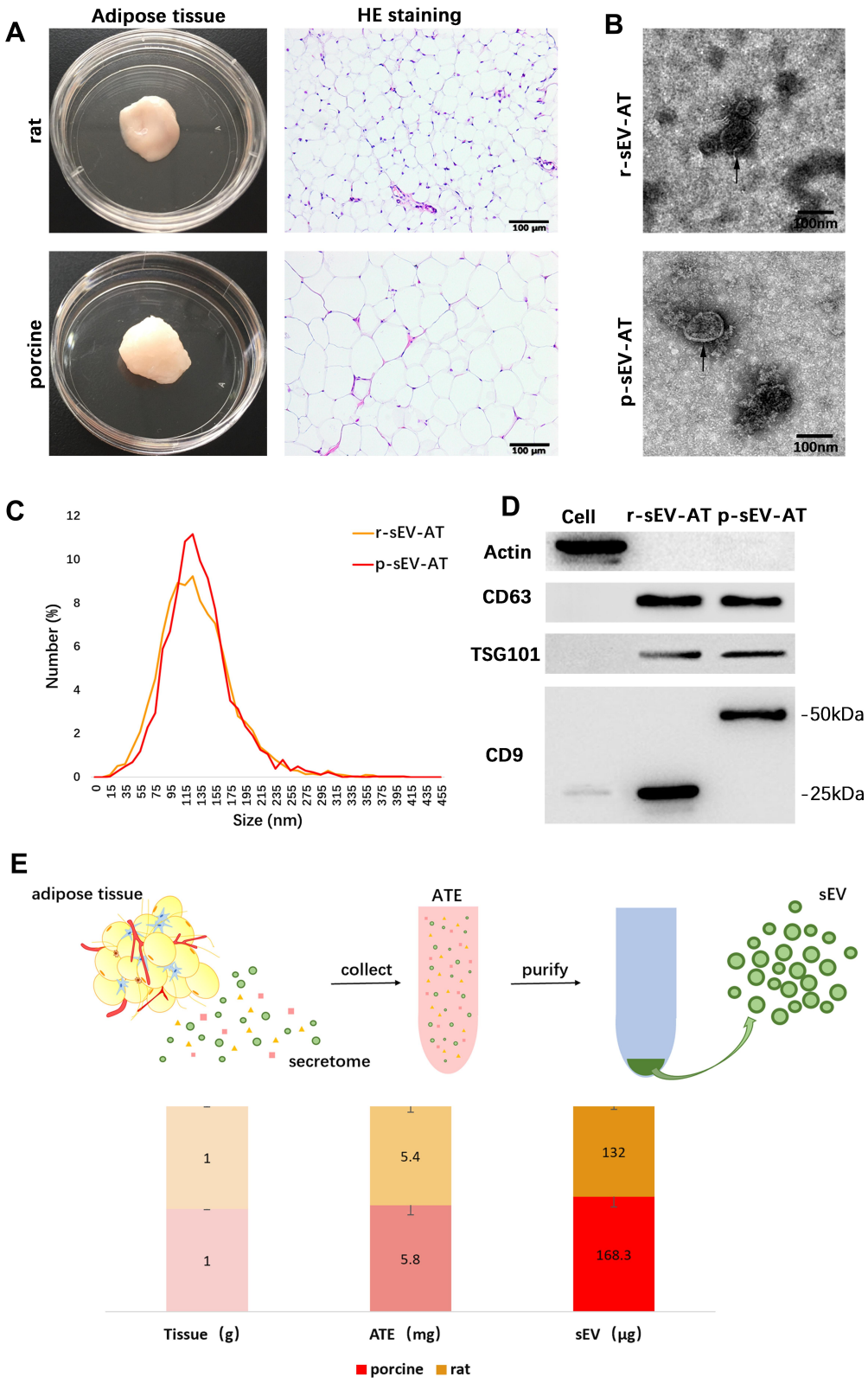

Figure 1 Characterization of r-sEV-AT and p-sEV-AT. (**A**) Macro and H&E images of native rat and porcine adipose tissue. Scale bar = 100 μm. (**B**) The morphology of r-sEV-AT and p-sEV-AT was observed by transmission electron microscopy analysis. The black arrows pointed out the sEV-AT. Scale bar = 100 nm. (**C**) Size distribution of sEV-AT was measured by NanoSight analysis. (**D**) The expressions of Actin, CD63, TSG101 and CD9 in cell debris, r-sEV-AT and p-sEV-AT were detected by Western blot. (**E**) The amount of ATE and sEV-AT that could be isolated from 1 g native adipose tissue (n=3).

Abbreviations: ATE, adipose tissue extract; H&E, hematoxylin and eosin; p-sEV-AT, small extracellular vesicles derived from porcine adipose tissue; r-sEV-AT, small extracellular vesicles derived from rat adipose tissue; sEV, small extracellular vesicles; sEV-AT, small extracellular vesicles derived from adipose tissue.

nm to 200 nm, and the average diameter was about 130 nm (Figure 1C). Western blot analysis confirmed the presence of sEV characteristic markers (CD9, CD63, and TSG101) in r-sEV-AT and p-sEV-AT. However, the presence of CD9 in r-sEV-AT was shown at different molecular weights compared to p-sEV-AT. The CD9 positive signal in r-sEV-AT was detected at 25kDa, but the presence of CD9 in p-sEV-AT was about 50kDa. The cellular protein actin was detected exclusively in the cell lysates (Figure 1D). These results confirmed that the source of adipose tissue and the size of adipocytes had little effect on the properties of sEV.

In order to compare the amount of sEV-AT that could be isolated from 1g adipose tissue (sEV/AT ratio), we selected the same amount of adipose tissue from rat and porcine, respectively, obtained adipose tissue extract (ATE) through suspension culture, and then purified sEV-AT from ATE, as described in our previous studies (Figure 1E).[25,26] Protein quantification is a common method to calculate the amount of sEV and tissue extract (TE). Therefore, the amount of obtained ATE and sEV-AT was determined by protein quantification. The results showed that the amount of r-ATE and p-ATE, respectively, obtained from 1g adipose tissue were similar, which showed to be 5.4 mg and 5.8 mg, respectively (Figure 1E). Then, we isolated r-sEV-AT and p-sEV-AT from 5.4 mg r-ATE and 5.8 mg p-ATE, respectively. The sEV/AT ratio of rat was about 132 μg/g, slightly lower than that of porcine, which showed to be 168.3 μg/g (Figure 1E). In general, the sEV/AT ratio of porcine was slightly higher than that of rat.

The Response of Cultured Cells to Allogeneic and Xenogeneic sEV-AT in vitro

rASCs and rECs were both isolated from SD rats and were adopted to evaluate the cellular response against allogeneic and xenogeneic sEV-AT in vitro. After co-cultured rASCs with r-sEV-AT and p-sEV-AT, respectively, we observed that rASCs could successfully uptake allogeneic and xenogeneic sEV-AT. In addition, there was no significant difference in the endocytosis ability of cells to allogeneic and xenogeneic sEV-AT (Figure 2A). In order to further study the effect of allogeneic and xenogeneic sEV-AT on cell differentiation. The expression levels of adipogenic marker gene (*PPARγ*, *C/EBPα*, *adiponectin* and *FABP4*) in the ASCs co-cultured with different sEV-AT were compared to the blank group. After cocultured for 5 days, the expressions of adipogenic marker genes in rASCs, were significantly higher than those in the blank group (Figure 2B). Except that the expression of *C/EBPα* induced by p-sEV-AT was higher than that induced by r-sEV-AT, other genes induced by sEV-AT derived from two species showed no difference. After co-cultured for 10 days, the expressions of *PPARγ* and *Adiponectin* in both r-sEV-AT and p-sEV-AT groups were upregulated to about 15-fold compared with the blank group. The expression of *FABP4* in r-sEV-AT and p-sEV-AT groups was upregulated to about 7-fold compared with the blank group (Figure 2C).

Angiogenesis played a vital role in soft tissue regeneration. In order to further evaluate the effect of allogeneic and xenogeneic sEV-AT on angiogenic differentiation of cells, rECs were induced by r-sEV-AT and p-sEV-AT for 4 days. Compared with the blank group, both r-sEV-AT and p-sEV-AT could promote tube-like structures formation, represented as the increasing of the total nodes, total junctions and total length. Besides, the inductivity of allogeneic and xenogeneic sEV-AT showed no difference (Figure 2D). The expressions of selected angiogenesis marker genes (*CD31*, *VEGF*, *FGF2*, and *angiogenin*) were also detected, the results showed 2- to 10-fold up-regulation in sEV-AT groups compared with the blank group (Figure 2E).

Taken together, sEV-AT derived from two species both could effectively induce the differentiation of rASCs or rECs, and the inductivity of allogeneic and xenogeneic sEV-AT showed no significant difference.

Host Cells Infiltration Induced by Allogeneic and Xenogeneic sEV-AT in vivo

In order to evaluate the response of host cells to allogeneic and xenogeneic sEV-AT in vivo, Matrigel only, or mixed with r-sEV-AT and p-sEV-AT was transferred into a custom-designed silicone tube, in which the cell-free implants only contacted the host cells through the upper and lower ends (Figure 3A). These mixtures were subcutaneously implanted into the back of SD rats. After 3D, 5D and 7D, the implants with the tubes were photographed (Figure 3A). Then, the tubes were removed and macro images showed that the implants contained r-sEV-AT and p-sEV-AT were opaque compared with the blank group at all time points (Figure 3B). We suspected that there might be more infiltrated host cells in sEV-AT groups which caused

the opaque appearances. To better compare the effect of host cells infiltration, we separated the implants at 3D, 5D and 7D, made paraffin sections, and selected sections that represented the center of the implants for HE staining. The lower edge of the sheet-like panniculus carnosus skeletal muscle[28] was defined as the starting point (solid line) and the position where the cell density significantly reduced was defined as the ending point (dotted line). The thickness between the solid line and the dotted line was used to evaluate the efficiency of the infiltration of host cells. As shown in the images from representative experiments, both the allogeneic and xenogeneic sEV-AT significantly promoted the infiltration of host cells at 5D and 7D (Figure 3C). After quantified over three independent studies, planimetry data showed that the average thickness in r-sEV-AT group at 5D and 7D were 633.25 μm and 1099.48 μm, respectively. In p-sEV-AT group, the average thickness was 704.19 μm at 5D and 1266.96 μm at 7D. These results indicated that chemotaxis host cell infiltration was accelerated by sEV-AT derived from two species. Moreover, there was no significant difference between allogeneic and xenogeneic sEV-AT groups at any time point (Figure 3D).

Neoadipose Tissue Formation Induced by Xenogeneic and Allogeneic sEV-AT in vivo

Our previous study has shown that sEV-AT derived from rat could be used as a cell-free therapeutic approach for adipose tissue regeneration. In order to systematically compare the effectiveness of xenogeneic and allogeneic sEV-AT in inducing neoadipose tissue regeneration, we evaluated neoadipose tissue formation after 2W, 4W and 8W of subcutaneous implantation. In general, we observed obvious blood vessels extending into the silicone tube in r-sEV-AT and p-sEV-AT groups, especially at 4W and 8W (Figure 4A). The implants in the blank group gradually absorbed with time, and only fine fibers remained at 8W. While the volume of regenerated tissue in allogeneic and xenogeneic sEV-AT groups at 4W and 8W were significantly larger than that in the blank group. (Figure 4B). To evaluate the area of neoadipose tissue, we calculated the area of immature or mature adipocyte by immunohistochemical staining (stained with adipocyte marker, perilipin A) so as to exclude the influence of unabsorbed Matrigel and fiber tissue (Figure 4C). We selected the sections in the middle of the silicone tube, the dotted line represented the area of neoadipose tissue (S1), the solid line represented the longitudinal section area of the silicone tube (S0), and S1/S0 represented the proportion of the neoadipose tissue in the silicone tube (Figure 4D). At 2W, immature adipocytes firstly appeared in p-sEV-AT but there was no statistical difference compared with the blank and r-sEV-AT groups. After 4W implantation, the average S1/S0 was 5.31% and 12.76% in r-sEV-AT and p-sEV-AT groups, respectively, which was higher than that of the blank group and showed significant difference, but there was no statistical difference between these two species. After 8W implantation, the average S1/S0 was 27.47% in r-sEV-AT group and 23.80% in p-sEV-AT group. In addition, regenerated adipose tissue in sEV-AT groups at 8W was close to the normal adipose tissue, which was accompanied by blood vessels to provide nutrition (Supplementary Figure S1). There was no significant difference in the area of neoadipose tissue induced by allogeneic and xenogeneic sEV-AT, but they were significantly higher than that of the blank group, in which there was a tiny adipocyte in the tubes (Figure 4E). These results indicated that the ability of xenogeneic sEV-AT to induce neoadipose tissue formation was not weaker than allogeneic sEV-AT in vivo.

Skin Wound Healing Accelerated by Allogeneic and Xenogeneic sEV-AT in vivo

To further compare the repair ability of allogeneic sEV-AT and xenogeneic sEV-AT in the soft tissue regeneration, a more complex soft tissue, like skin, was considered. The skin is not only the largest and most important barrier structure of the human body[29] but also very complex in the microstructure. The dermis contains fibroblasts, adipocytes, hair follicles, sweat glands, blood vessels, fibers and so on.[28] Besides, the regeneration of epidermis is always a question of great concern in the field of skin repair.

In our study, full-thickness dermal wounds (15 mm in diameter) were generated on the back of SD rats, and then r-sEV-AT and p-sEV-AT mixed with Polyvinyl Alcohol (PVA) were dropped onto the surface of the wound. For the blank group, an equal volume of PBS mixed with 200 μL PVA was directly dropped onto the surface of each wound. Wound areas were photographed at 0D, 7D, 10D, 14D, 21D to determine

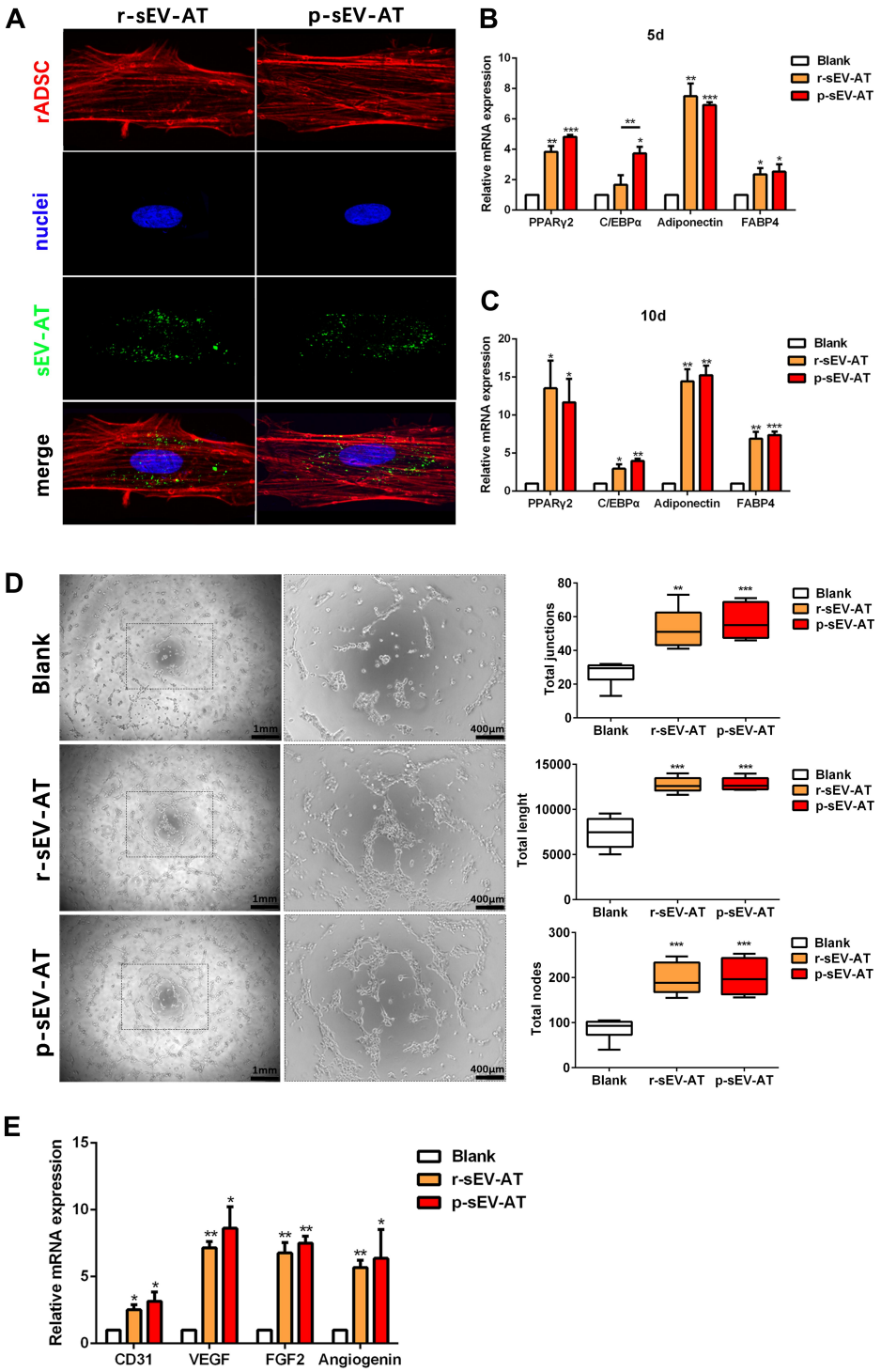

Figure 2 The response of cultured cells to allogeneic and xenogeneic sEV-AT in vitro. (**A**) The morphology of rASCs and cellular uptake were detected by Fluorescence Confocal Microscopy (red: rASCs, green: sEV-AT, blue: nuclei). After co-cultured rASCs with sEV-AT for (**B**) 5 days or (**C**) 10 days, the relative expressions of adipogenic marker genes (*PPARγ*, *C/EBPα*, *adiponectin* and *FABP4*) were measured by real-time PCR (n=3). (**D**) Typical tube-like structures of rECs in different groups were shown (left, scar bar=1 mm, right, scar bar=400 μm), and total nodes, total junctions and total length of all tubing per field of view (scar bar=500 μm) were analyzed (n=5). (**E**) After co-cultured rECs with sEV-AT for 4 days, the relative expressions of angiogenic marker genes (*CD31*, *VEGF*, *FGF2* and *angiogenin*) were measured by real-time PCR (n=3). The significance was tested with one-way ANOVA with Tukey posthoc test (*p<0.05, **p<0.01, ***p <0.001).

Abbreviations: *C/EBPα*, *CCAAT enhancer-binding proteins; FABP4, fatty acid-binding protein 4*; *FGF2*, *fibroblast growth factor 2; PCR, polymerase chain reaction*; *PPARγ*, *peroxisome proliferator-activated receptor γ*; p-sEV-AT, small extracellular vesicles derived from porcine adipose tissue; rASCs, rat adipose-derived stromal/stem cells; rECs, rat aorta endothelial cells; r-sEV-AT, small extracellular vesicles derived from rat adipose tissue; sEV-AT, small extracellular vesicles derived from adipose tissue; *VEGF, vascular endothelial growth factor.*

wound closure rate (Figure 5A). In order to show the speed of wound healing more clearly, we made a pattern map which was similar to the contour to show the area of unhealed wounds at different time points (Figure 5B). As shown in the images from representative experiments and wound traces, the wounds in r-sEV-AT and p-sEV-AT groups consistently closed faster than that in the blank group (Figure 5A and B). When quantified over three independent wound studies, the biggest difference of the area of unhealed between in sEV-AT groups and in the blank group was at 10D post-wounding. Planimetry data showed that the average wound area in allogeneic and xenogeneic groups was significantly shrunk to about 20%, which showed to be about 60% in the blank group (Figure 5C). Importantly, no significant difference in the wound healing process was observed between wounds treated with r-sEV-AT and p-sEV-AT at any time point.

Re-Epithelialization, Granulation Tissue and Hair Follicles Improved by Allogeneic and Xenogeneic sEV-AT in vivo

Having confirmed that both r-sEV-AT and p-sEV-AT accelerated the wound healing process from gross observation, we therefore wondered whether r-sEV-AT or p-sEV-AT could provide a favorable microenvironment to speed up the restoration of epidermal and dermal architecture. Next, histological analysis was performed to assess the effect of allogeneic and xenogeneic sEV-AT on skin wound healing in the microstructure.

To visualize the degree of re-epithelialization, the thickness of granulation tissue formation and hair follicle regeneration, wounded skins were collected at 10D followed by H&E staining (Figure 6A and B). We used black inverted triangles to mark the edge of the original wound and used red inverted triangles to represent the edge of re-epithelization (Figure 6A). The edge of re-epithelization theoretically represented the edge of the unhealed wounds which is depicted in Figure 5A and B. At the same time, the orange star represented the disordered wound area, which was composed of irregular scab shell and granulation tissue (Figure 5A). An epithelial tongue of migrating keratinocytes was visible clearly in each group (Figure 6B). Compared with the blank group, wound re-epithelialization was remarkably enhanced after treatment with allogeneic and xenogeneic sEV-AT (Figure 6A and C). Moreover, sEV-AT treatment significantly improved the thickness of regularly arranged granulation tissue compared to the blank group (Figure 6D), which suggested that there were more capillaries in wound beds treated with allogeneic and xenogeneic sEV-AT. In addition, we observed regenerated hair follicles in the repaired skin area in r-sEV-AT and p-sEV-AT groups, which were pointed out by black arrows (Figure 6A). Although we did not quantitatively analyze the number of regenerated hair follicles, there was no obvious hair follicle structure in the blank group (Figure 6A), which also proved the ability of allogeneic and xenogeneic sEV-AT to promote complex soft tissue regeneration. In short, these results indicated that r-sEV-AT or p-sEV-AT significantly promoted wound re-epithelialization, granulation formation and hair follicle regeneration and thus accelerated skin wound healing.

Discussion

In recent years, a great deal of attention has been paid to the application of not only allogeneic but also xenogeneic sEV in various fields, such as therapeutic target,[30–32] diagnosis tools,[33] drug/gene delivery vector[34] and inducer of tissue regeneration.[35–37] Although the highly attractive features of sEV, such as the absence of immunogenicity, natural composition, and the ability to be loaded with small molecules and biologics,[38] the use of sEV derived from xenogeneic tissue in clinical applications remained limited because it was still unclear whether sEV derived from different species would have an impact on their therapeutic effects.

In our experiments, we successfully isolated r-sEV-AT and p-sEV-AT from rat and porcine adipose tissue, respectively. Although the size of adipocytes from rat and porcine was quite different, the physical characteristics of sEV-AT derived from two species assessed by TEM and Nanosight revealed no significant difference in what concerning shape, size and size distribution. Western blot analysis indicated that both r-sEV-AT and p-sEV-AT expressed the marker proteins, CD9, CD63 and TSG101. However, CD9 positive signal in r-sEV-AT was detected at 25kDa, but the presence of CD9 in p-sEV-AT was about 50kDa, in which CD9 might be detected as a dimer. We also found that the sEV/AT ratio of porcine was slightly higher than that of rat. Adipose tissue consists of cellular components, such as adipocytes, preadipocytes, ASCs, endothelial cells,

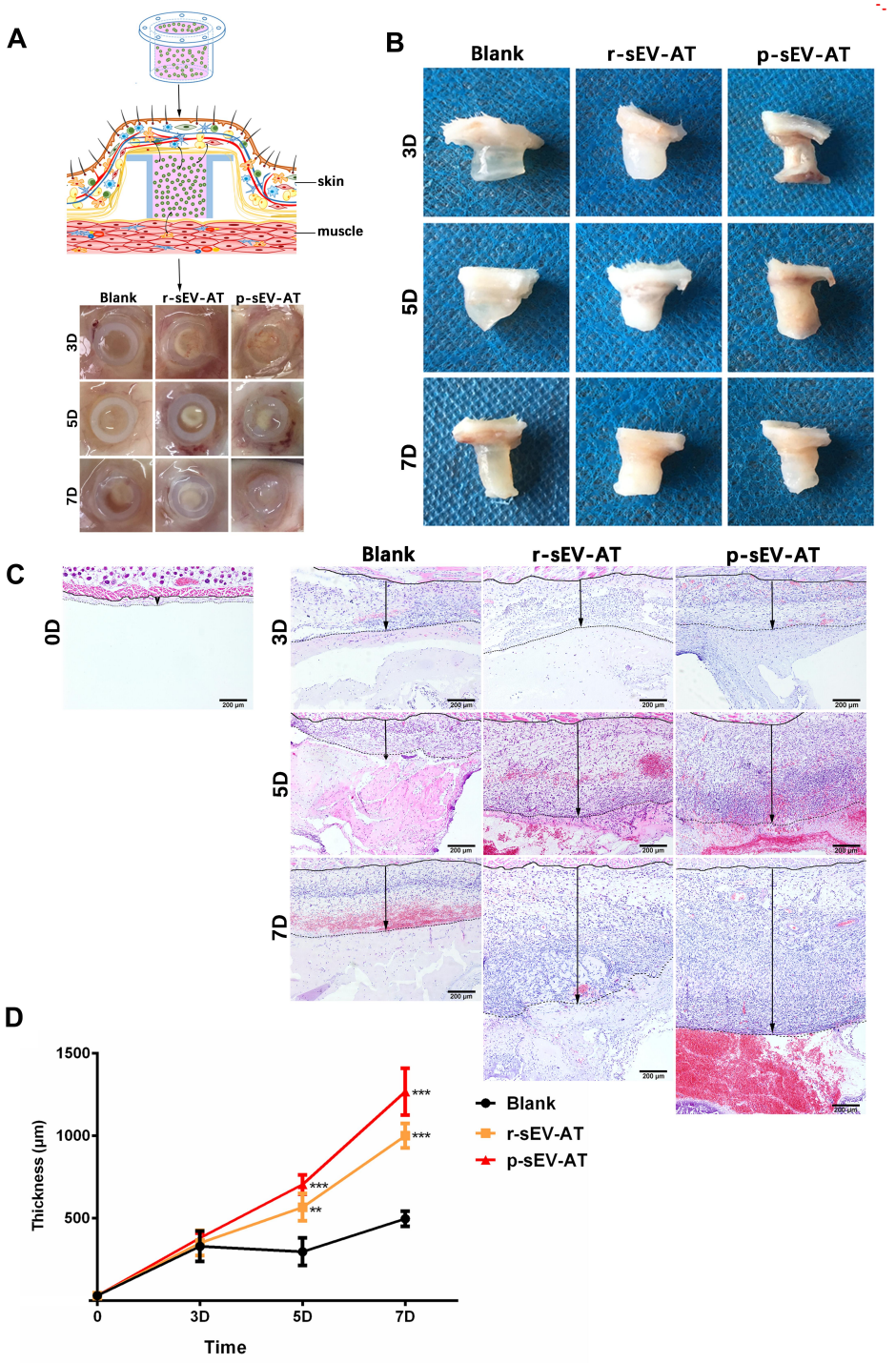

Figure 3 Host cells infiltration induced by allogeneic and xenogeneic sEV-AT in vivo. Host cells infiltration in tubes was measured at 3D, 5D and 7D. (**A**) Schematic view of the experimental operation process. Matrigel only, or mixed with r-sEV-AT and p-sEV-AT was transferred into the custom-designed silicone tube and subcutaneously implanted it into the back of SD rats. After 3D, 5D and 7D implantation, samples with the tubes were photographed. (**B**) Macro images of the implants after removing the tubes. (**C**) Host cells infiltration was confirmed by H&E staining. The solid lines represented the lower edge of the sheet-like panniculus carnosus skeletal muscle in the skin, the dotted lines represented the position where the cell density is significantly reduced and the black arrows represented the thickness of cell infiltration. Scale bar = 200 μm. (**D**) The average thickness of cells infiltration in different groups (n=3). The significance was tested with one-way ANOVA with Tukey posthoc test (**p<0.01, ***p <0.001).

Abbreviations: p-sEV-AT, small extracellular vesicles derived from porcine adipose tissue; r-sEV-AT, small extracellular vesicles derived from rat adipose tissue; sEV-AT, small extracellular vesicles.

fibroblasts, keratinocytes, macrophages and smooth muscle cells, and acellular components, extracellular matrix (ECM).[39] Previous study has shown that sEV were almost secreted by active cells.[40] Our study showed that adipocytes of porcine were larger than those of rat and the relative proportion of extracellular matrix of porcine was little, so we speculated that there were more active cells per unit mass of adipose tissue in porcine than in rat.

Firstly, the uptake of sEV by target cells was the premise of regulation.[41] Several mechanisms have been involved in sEV uptake by target cells, including protein interactions, endocytosis, cell surface membrane fusion and cell-specific sEV uptake.[15] In our study, we co-cultured rASCs with r-sEV-AT or p-sEV-AT, and the result showed that the uptake of allogeneic and xenogeneic sEV-AT by rASCs showed no significant difference. Although there was a specific protein-protein recognition mechanism in sEV uptake,[42] we speculated that in the process of uptake, non-specific processes, such as endocytosis[43] and cell surface membrane fusion,[44] might play a large role.

In the process of soft tissue repair, the commitment and remodeling of mesenchymal stromal cells and endothelial cells was an important process. In order to systematically compare the effectiveness of allogeneic and xenogeneic sEV on the commitment of cultured cells, we evaluated the adipogenic differentiation of rASCs and the angiogenic differentiation of rECs induced by r-sEV-AT and p-sEV-AT. Our results indicated that sEV had no species difference in inducing the differentiation of cultured cells. This might be related to the complexity of the regulatory mechanism of cell differentiation. We have known that many proteins[45,46] and a lot of miRNAs[25,47-51] have been reported to participate in adipogenic differentiation. Similarly, for angiogenesis, both proteins[52–57] and miRNAs[58–60] played a regulatory role. Due to the complexity of regulatory pathways, we speculated that species-specific proteins and pathways would be replaced by other species-nonspecific pathways. In addition to thousands of proteins carried by sEV, a large number of miRNAs have been identified in sEV and been reported to play a critical role in the regulation of cell differentiation.[61] These miRNAs were generally conserved in evolution, even about 70% miRNAs conserved in mammals.[62] Therefore, a part of regulatory role of miRNAs might be another reason why there was no significant difference in cell differentiation induced by allogeneic and xenogeneic sEV. However, whether species-nonspecific proteins and miRNAs play a major role in regulating cell differentiation needed to be investigated in further study.

The injury induced by the surgical procedure of implantation always initiates a cascade of host responses. During the initial acute inflammatory response, neutrophils and monocytes are recruited to the site of injured site, may lead to restoration of tissue integrity, finally repaired tissue defect.[63] Therefore, whether host cells successfully migrated to the injured site and the migration speed were the key parts of tissue repair. In order to compare the effect of allogeneic and xenogeneic sEV on host cell migration, we specially designed a silicone tube, in which the cell-free implants only contacted the host cells through the upper and lower ends. We found that sEV derived from two species could significantly promote the migration of host cells compared with the blank group at early implantation stage, which might lead to elevated neoadipose tissue formation in silicone tube at 8 weeks post implantation. Up to now, immune response induced by xenografts have been reported mainly at the organ[64] and cellular[65] levels, but no study focuses on xenogeneic extracellular vesicle. In this study, although host cells recruitment caused by implantation were promoted in sEV-AT groups, there was no significant difference between allogeneic and xenogeneic sEV-AT groups. Our results indicated that xenogeneic sEV did not cause specific inflammatory response, which confirmed that sEV was a kind of bioactive material with low immunogenicity.

The skin is the largest organ of the human body, and had relatively complex structures, such as dermis, epidermis, hair follicles, sweat glands and so on.[29] In recent years, some studies applied allogeneic sEV in skin wound healing and even compared the effectiveness of sEV from different cell sources. For example, Pelizzo G et al compared the effect of sEV derived from rabbit adipose stromal cells (ASC-sEV) and rabbit bone marrow cells (BM-sEV) on rabbit cutaneous wound healing. The results showed that these two kinds of sEV accelerated skin wound healing and ASC-sEV-treated wounds were significantly better than BM-sEVs.[66] Some others focused on the effect of xenogeneic sEV in skin wound healing. For example, Zhang, W et al found that injection of exosomes derived from human ASCs accelerated full-thickness skin wound healing and attenuated scar

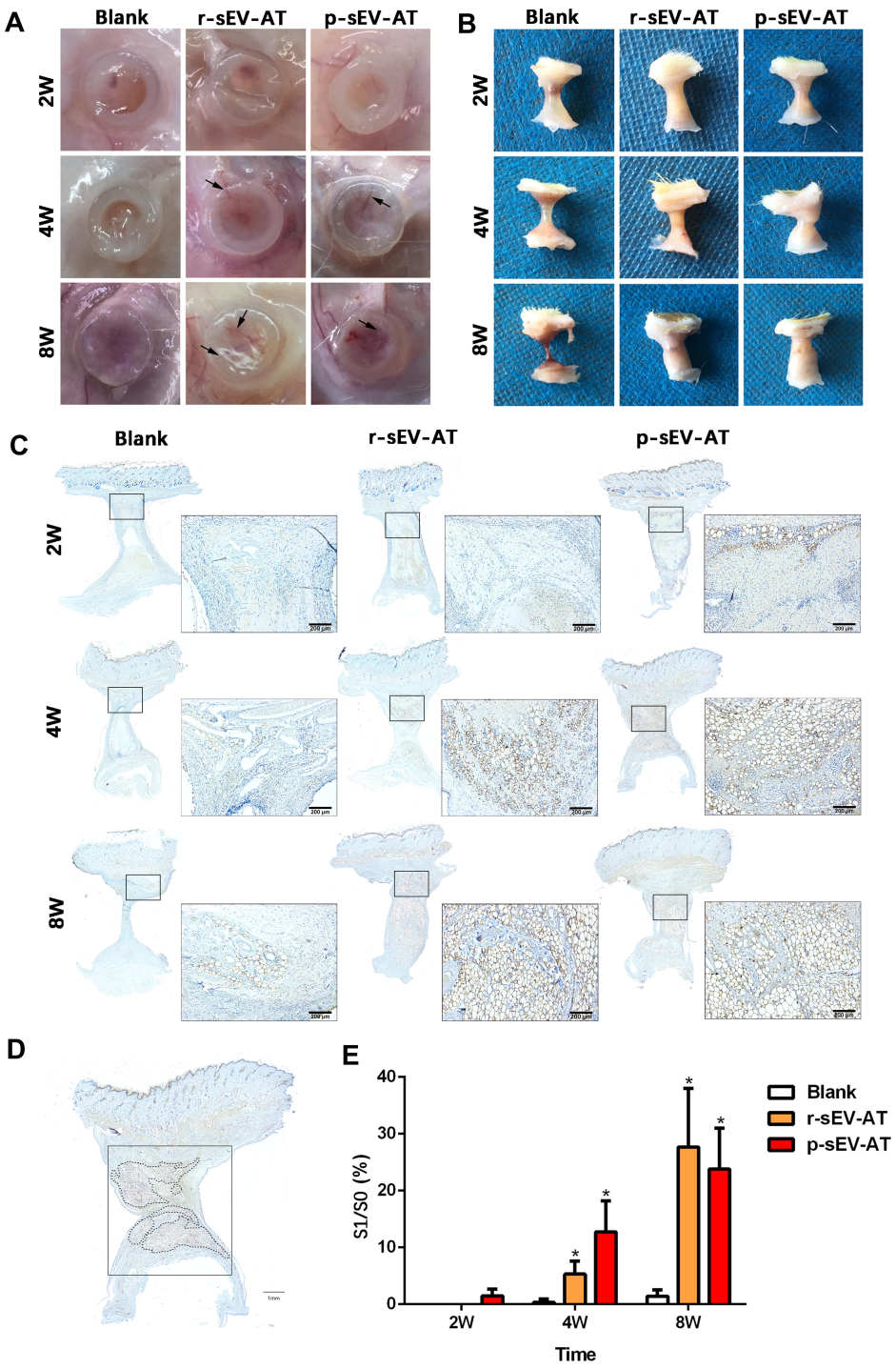

Figure 4 Neoadipose tissue formation induced by xenogeneic and allogeneic sEV-AT in vivo. Macro images of the implants (**A**) with the tubes or (**B**) without the tubes in the blank, r-sEV-AT and p-sEV-AT groups at 2W, 4W and 8W. The black arrows pointed out the blood vessels. (**C**) Immature and mature adipocytes were confirmed by immunohistochemical staining (stained with adipocyte marker, perilipin A). Scale bar = 200 μm. (**D**) Selected sections represented the center of the implants, the dotted line represented the area of neoadipose tissue (S1), the solid line represented the longitudinal section area of the silicone tube (S0), and S1/S0 represented the proportion of the neoadipose tissue in the silicone tube. (**E**) The average of S1/S0 in different groups (n=3). The significance was tested with one-way ANOVA with Tukey posthoc test (*$p<0.05$).

Abbreviations: p-sEV-AT, small extracellular vesicles derived from porcine adipose tissue; r-sEV-AT, small extracellular vesicles derived from rat adipose tissue; sEV-AT, small extracellular vesicles derived from adipose tissue.

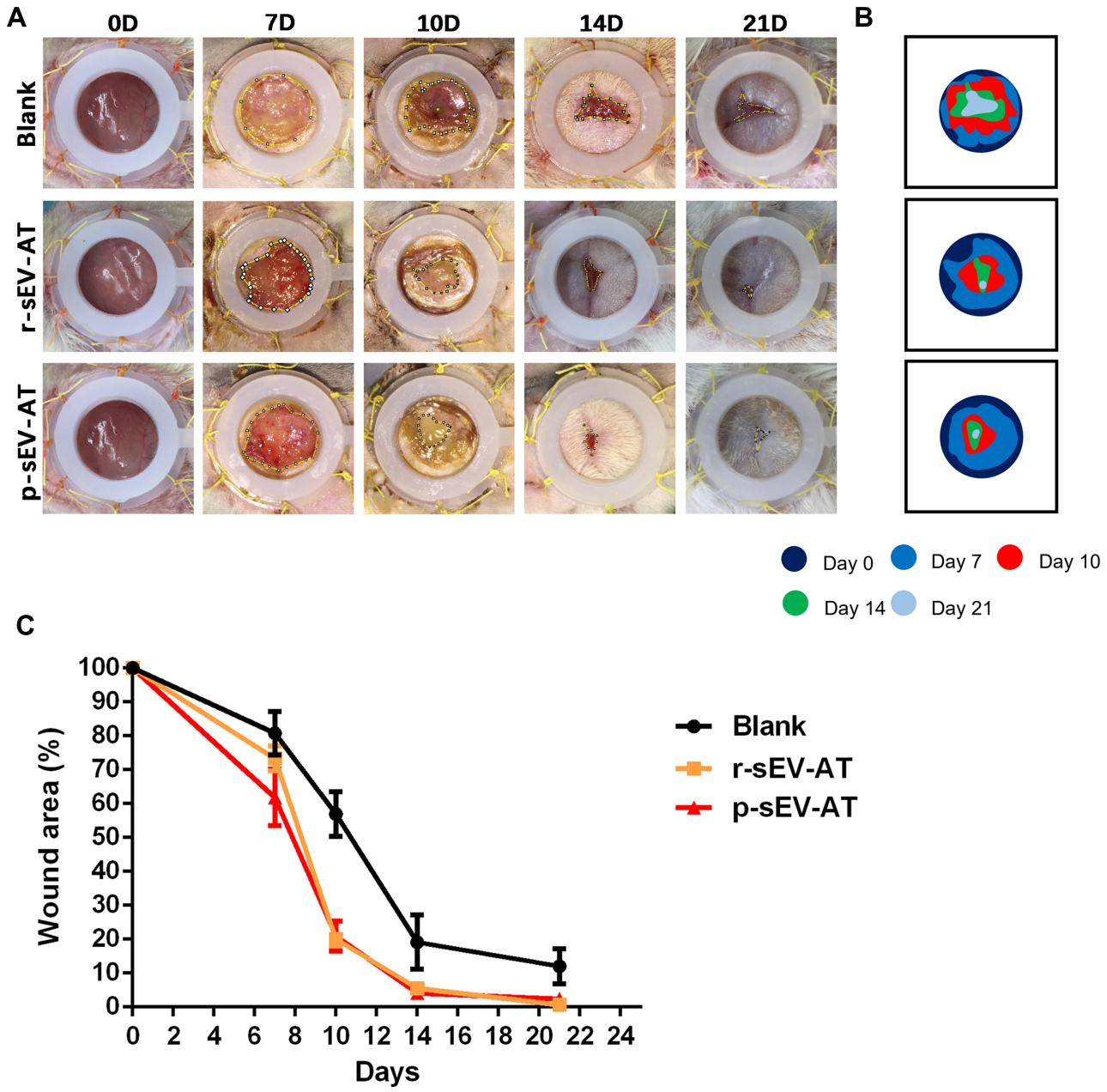

Figure 5 Skin wound healing accelerated by allogeneic and xenogeneic sEV-AT. (**A**) Macro images of skin wounds at 0D, 7D, 10D,14D and 21D. (**B**) From these images, wound edge traces were established for each time point. (**C**) Quantification of the wound area from 0D to 21D (n=3).
Abbreviations: p-sEV-AT, small extracellular vesicles derived from porcine adipose tissue; r-sEV-AT, small extracellular vesicles derived from rat adipose tissue; sEV-AT, small extracellular vesicles derived from adipose tissue.

formation in mice.[67] However, there was no article focused on the different effect of allogeneic and xenogeneic sEV on skin wound repair. To solve this puzzle, we created a full-thickness skin defect model and dropped sEV derived from two species on the wound. By comparison of macro and microstructure, we found that both allogeneic and xenogeneic sEV-AT accelerated skin wound healing and significantly induced re-epithelialization, granulation tissue formation and hair follicles regeneration. Notably, for this complex soft tissue repair, the effectiveness of allogeneic and xenogeneic sEV was almost the same. These results indicated that sEV from the same tissue carried similar content which played a role in soft tissue regeneration and species might not be the main factor for sEV function.

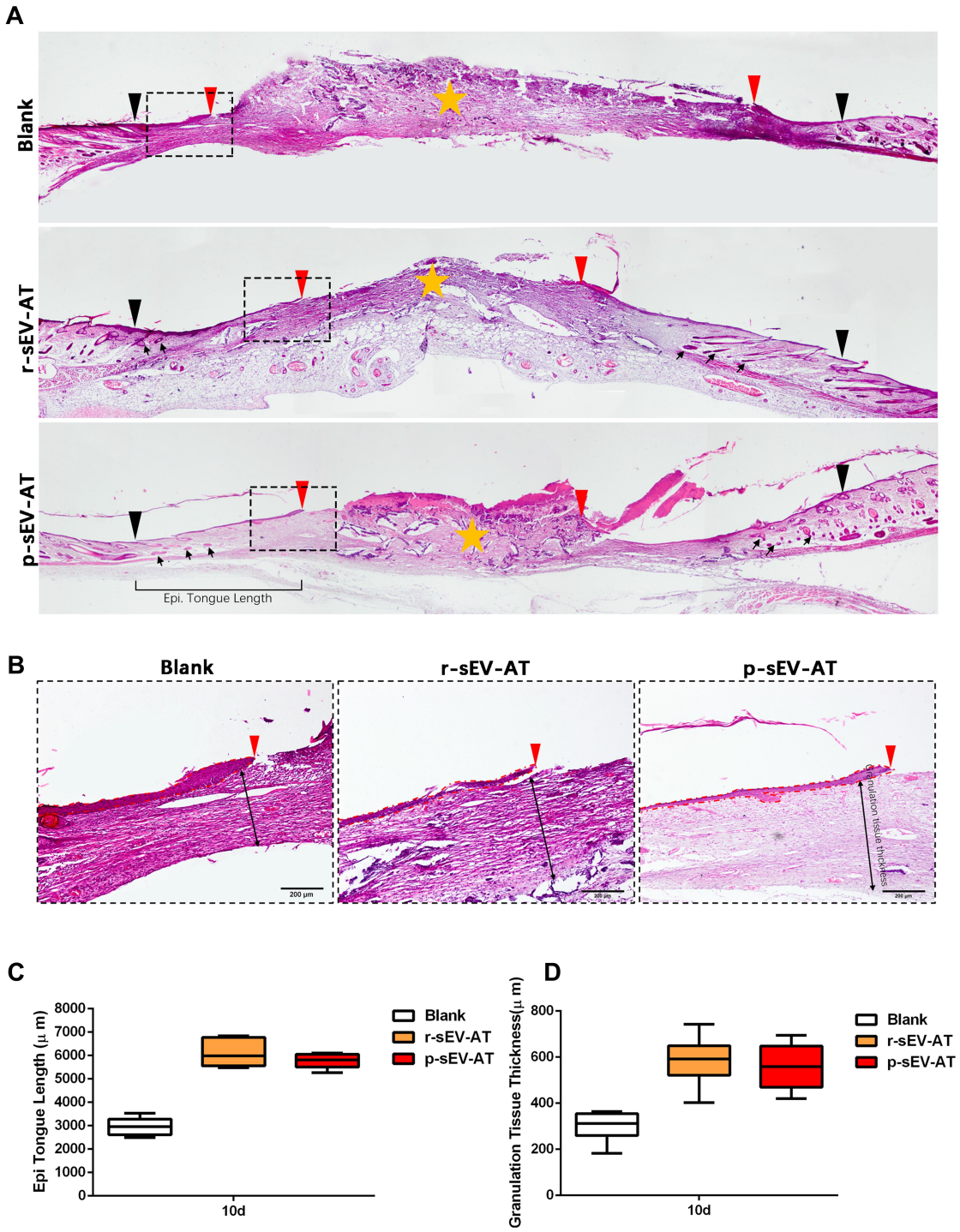

Figure 6 Skin wound healing in microstructure was improved by allogeneic and xenogeneic sEV-AT. (**A**) The microstructure of skin wounds at 10D was investigated by H&E staining. The black inverted triangles pointed out the original wound edges; the red inverted triangles pointed out the edge of re-epithelization; the black arrows pointed out the regenerated hair follicles; the orange star pointed out the disordered wound area. Magnified panels (**B**) the red inverted triangles pointed out the edge of re-epithelization; the dotted red lines pointed out the area of regenerated epithelium; the black two-way arrows pointed out the thickness of regularly arranged granulation tissue. Scale bar = 200 μm. (**C**) Quantification of the length of regenerated epidermal tongue at 10D. (**D**) Quantification of the thickness of granulation tissue at 10D (n=3). **Abbreviations**: H&E, hematoxylin and eosin; p-sEV-AT, small extracellular vesicles derived from porcine adipose tissue; r-sEV-AT, small extracellular vesicles derived from rat adipose tissue; sEV-AT, small extracellular vesicles derived from adipose tissue.

Conclusion

The previous results demonstrated that the low immunogenicity of sEV was to make xenogeneic applications possible, but whether there were differences in the therapeutic effects of different species was still confusing. Our work, for the first time, systematically compares the characteristics of sEV derived from different species and the effectiveness of allogeneic and xenogeneic sEV-AT on soft tissue regeneration. The results showed the ability of allogeneic and xenogeneic sEV-AT on promoting soft tissue regeneration was similar. Considering the abundant sources, high yield and guaranteed effectiveness, porcine adipose tissue-derived sEV appeared to be a potential raw material for further application.

Author Contributions

All authors made substantial contributions to conception and design, acquisition of data, or analysis and interpretation of data; took part in drafting the article or revising it critically for important intellectual content; gave final approval of the version to be published; and agree to be accountable for all aspects of the work.

Funding

This work was supported by the National Key R&D Program of China (2017YFA0104800) and Key Technology R&D Program of Sichuan Province (2019YFS0312).

Disclosure

All authors reported no conflicts of interest in this work.

References

1. Mathieu M, Martin-Jaular L, Lavieu G, Théry C. Specificities of secretion and uptake of exosomes and other extracellular vesicles for cell-to-cell communication. *Nat Cell Biol*. 2019;21(1):9–17. doi:10.1038/s41556-018-0250-9
2. Théry C, Regnault A, Garin J, et al. Molecular characterization of dendritic cell-derived exosomes. Selective accumulation of the heat shock protein hsc73. *J Cell Biol*. 1999;147(3):599–610. doi:10.1083/jcb.147.3.599
3. Kato-Yoshinaga Y, Nagano M, Mori S, Clare A, Fusetani N, Matsumura K. Species specificity of barnacle settlement-inducing proteins. *Comp Biochem Physiol A Mol Integr Physiol*. 2000;125(4):511–516. doi:10.1016/S1095-6433(00)00179-3
4. Katsuura Y, Mochizuki T, Tamura M, et al. Species specificity of anticoagulant activity of activated human protein C: involvement of factor V as well as protein S. *Thromb Res*. 1996;82(2):147–157. doi:10.1016/0049-3848(96)00061-8
5. Sorokin L, Morgan E. Species specificity of transferrin binding, endocytosis and iron internalization by cultured chick myogenic cells. *J Comp Physiol B*. 1988;158(5):559–566. doi:10.1007/BF00692564
6. Druz A, Chu C, Majors B, Santuary R, Betenbaugh M, Shiloach J. A novel microRNA mmu-miR-466h affects apoptosis regulation in mammalian cells. *Biotechnol Bioeng*. 2011;108(7):1651–1661. doi:10.1002/bit.23092
7. Tang R, Li L, Zhu D, et al. Mouse miRNA-709 directly regulates miRNA-15a/16-1 biogenesis at the posttranscriptional level in the nucleus: evidence for a microRNA hierarchy system. *Cell Res*. 2012;22(3):504–515. doi:10.1038/cr.2011.137
8. Medeiros L, Dennis L, Gill M, et al. Mir-290-295 deficiency in mice results in partially penetrant embryonic lethality and germ cell defects. *Proc Natl Acad Sci U S A*. 2011;108(34):14163–14168. doi:10.1073/pnas.1111241108
9. Mor E, Cabilly Y, Goldshmit Y, et al. Species-specific microRNA roles elucidated following astrocyte activation. *Nucleic Acids Res*. 2011;39(9):3710–3723. doi:10.1093/nar/gkq1325
10. Grün D, Wang YL, Langenberger D, Gunsalus KC, Rajewsky N. microRNA target predictions across seven drosophila species and comparison to mammalian targets. *PLoS Comput Biol*. 2005;1(1):e13. doi:10.1371/journal.pcbi.0010013
11. Lall S, Grün D, Krek A, et al. A genome-wide map of conserved microRNA targets in C. elegans. *Curr Biol*. 2006;16(5):460–471. doi:10.1016/j.cub.2006.01.050
12. Mayr C, Hemann MT, Bartel DP. Disrupting the pairing between let-7 and Hmga2 enhances oncogenic transformation. *Science*. 2007;315(5818):1576–1579. doi:10.1126/science.1137999
13. Lee CT, Risom T, Strauss WM. Evolutionary conservation of microRNA regulatory circuits: an examination of microRNA gene complexity and conserved microRNA-target interactions through metazoan phylogeny. *DNA Cell Biol*. 2007;26(4):209–218. doi:10.1089/dna.2006.0545
14. Yáñez-Mó M, Siljander P, Andreu Z, et al. Biological properties of extracellular vesicles and their physiological functions. *J Extracell Vesicles*. 2015;4(1):27066. doi:10.3402/jev.v4.27066
15. van Niel G, D'Angelo G, Raposo G. Shedding light on the cell biology of extracellular vesicles. *Nat Rev Mol Cell Biol*. 2018;19(4):213–228.
16. Valadi H, Ekström K, Bossios A, Sjöstrand M, Lee J, Lötvall J. Exosome-mediated transfer of mRNAs and microRNAs is a novel mechanism of genetic exchange between cells. *Nat Cell Biol*. 2007;9(6):654–659. doi:10.1038/ncb1596
17. Flaherty S, Grijalva A, Xu X, Ables E, Nomani A, Ferrante A. A lipase-independent pathway of lipid release and immune modulation by adipocytes. *Science*. 2019;363(6430):989–993. doi:10.1126/science.aaw2586
18. Buschow S, Liefhebber J, Wubbolts R, Stoorvogel W. Exosomes contain ubiquitinated proteins. *Blood Cells Mol Dis*. 2005;35(3):398–403. doi:10.1016/j.bcmd.2005.08.005
19. Tseliou E, Fouad J, Reich H, et al. Fibroblasts rendered antifibrotic, antiapoptotic, and angiogenic by priming with cardiosphere-derived extracellular membrane vesicles. *J Am Coll Cardiol*. 2015;66(6):599–611. doi:10.1016/j.jacc.2015.05.068
20. Ibrahim A, Cheng K, Marbán E. Exosomes as critical agents of cardiac regeneration triggered by cell therapy. *Stem Cell Rep*. 2014;2(5):606–619. doi:10.1016/j.stemcr.2014.04.006
21. Gallet R, Dawkins J, Valle J, et al. Exosomes secreted by cardiosphere-derived cells reduce scarring, attenuate adverse remodelling, and improve function in acute and chronic porcine myocardial infarction. *Eur Heart J*. 2017;38(3):201–211. doi:10.1093/eurheartj/ehw240
22. Ailhaud G. Adipose tissue as a secretory organ: from adipogenesis to the metabolic syndrome. *C R Biol*. 2006;329(8):570–577. doi:10.1016/j.crvi.2005.12.012
23. Sorisky A, Molgat AS, Gagnon A. Macrophage-induced adipose tissue dysfunction and the preadipocyte: should I stay (and differentiate) or should I go? *Adv Nutr*. 2013;4(1):67–75. doi:10.3945/an.112.003020

24. Crewe C, Joffin N, Rutkowski JM, et al. An endothelial-to-adipocyte extracellular vesicle axis governed by metabolic state. *Cell*. 2018;175(3):695–708 e613. doi:10.1016/j.cell.2018.09.005
25. Zhang Y, Yu M, Dai M, et al. miR-450a-5p within rat adipose tissue exosome-like vesicles promotes adipogenic differentiation by targeting WISP2. *J Cell Sci*. 2017;130(6):1158–1168. doi:10.1242/jcs.197764
26. Dai M, Yu M, Zhang Y, Tian W. Exosome-like vesicles derived from adipose tissue provide biochemical cues for adipose tissue regeneration. *Tissue Eng Part A*. 2017;23(21–22):1221–1230. doi:10.1089/ten.tea.2017.0045
27. Tian H, Suo N, Li F, Yang C, Qiong X. An effective method of isolating endothelial cells from intact rat aorta. *Cell Biochem Biophys*. 2014;70(1):423–427. doi:10.1007/s12013-014-9933-4
28. Rivera-Gonzalez G, Shook B, Horsley V. Adipocytes in skin health and disease. *Cold Spring Harb Perspect Med*. 2014;4(3):a015271–a015271. doi:10.1101/cshperspect.a015271
29. Proksch E, Brandner J, Jensen J. The skin: an indispensable barrier. *Exp Dermatol*. 2008;17(12):1063–1072. doi:10.1111/j.1600-0625.2008.00786.x
30. Xie F, Zhou X, Fang M, et al. Extracellular vesicles in cancer immune microenvironment and cancer immunotherapy. *Adv Sci (Weinh)*. 2019;6(24):1901779.
31. Barile L, Vassalli G. Exosomes: therapy delivery tools and biomarkers of diseases. *Pharmacol Ther*. 2017;174:63–78. doi:10.1016/j.pharmthera.2017.02.020
32. Bei Y, Das S, Rodosthenous RS, et al. Extracellular vesicles in cardiovascular theranostics. *Theranostics*. 2017;7(17):4168–4182. doi:10.7150/thno.21274
33. Rahbarghazi R, Jabbari N, Sani NA, et al. Tumor-derived extracellular vesicles: reliable tools for cancer diagnosis and clinical applications. *Cell Commun Signal*. 2019;17(1):73. doi:10.1186/s12964-019-0390-y
34. Wang S, Gao J, Wang Z. Outer membrane vesicles for vaccination and targeted drug delivery. *Wiley Interdiscip Rev Nanomed Nanobiotechnol*. 2019;11(2):e1523. doi:10.1002/wnan.1523
35. Trubiani O, Marconi GD, Pierdomenico SD, Piattelli A, Diomede F, Pizzicannella J. Human oral stem cells, biomaterials and extracellular vesicles: a promising tool in bone tissue repair. *Int J Mol Sci*. 2019;20(20):4987. doi:10.3390/ijms20204987
36. Trubiani O, Pizzicannella J, Caputi S, et al. Periodontal ligament stem cells: current knowledge and future perspectives. *Stem Cells Dev*. 2019;28(15):995–1003. doi:10.1089/scd.2019.0025
37. Henriques-Antunes H, Cardoso RMS, Zonari A, et al. The kinetics of small extracellular vesicle delivery impacts skin tissue regeneration. *ACS Nano*. 2019;13(8):8694–8707. doi:10.1021/acsnano.9b00376
38. Garofalo M, Villa A, Rizzi N, et al. Extracellular vesicles enhance the targeted delivery of immunogenic oncolytic adenovirus and paclitaxel in immunocompetent mice. *J Control Release*. 2019;294:165–175. doi:10.1016/j.jconrel.2018.12.022
39. Zuk PA, Zhu M, Ashjian P, et al. Human adipose tissue is a source of multipotent stem cells. *Mol Biol Cell*. 2002;13(12):4279–4295. doi:10.1091/mbc.e02-02-0105
40. Johnstone RM, Adam M, Hammond JR, Orr L, Turbide C. Vesicle formation during reticulocyte maturation. Association of plasma membrane activities with released vesicles (exosomes). *J Biol Chem*. 1987;262(19):9412–9420.
41. Tian T, Wang Y, Wang H, Zhu Z, Xiao Z. Visualizing of the cellular uptake and intracellular trafficking of exosomes by live-cell microscopy. *J Cell Biochem*. 2010;111(2):488–496. doi:10.1002/jcb.22733
42. Christianson HC, Svensson KJ, van Kuppevelt TH, Li JP, Belting M. Cancer cell exosomes depend on cell-surface heparan sulfate proteoglycans for their internalization and functional activity. *Proc Natl Acad Sci U S A*. 2013;110(43):17380–17385. doi:10.1073/pnas.1304266110
43. Morelli AE, Larregina AT, Shufesky WJ, et al. Endocytosis, intracellular sorting, and processing of exosomes by dendritic cells. *Blood*. 2004;104(10):3257–3266. doi:10.1182/blood-2004-03-0824
44. Parolini I, Federici C, Raggi C, et al. Microenvironmental pH is a key factor for exosome traffic in tumor cells. *J Biol Chem*. 2009;284(49):34211–34222. doi:10.1074/jbc.M109.041152
45. Lin FT, Lane MD. CCAAT/enhancer binding protein alpha is sufficient to initiate the 3T3-L1 adipocyte differentiation program. *Proc Natl Acad Sci U S A*. 1994;91(19):8757–8761. doi:10.1073/pnas.91.19.8757
46. Chawla A, Schwarz EJ, Dimaculangan DD, Lazar MA. Peroxisome proliferator-activated receptor (PPAR) gamma: adipose-predominant expression and induction early in adipocyte differentiation. *Endocrinology*. 1994;135(2):798–800. doi:10.1210/endo.135.2.8033830
47. Esau C, Kang X, Peralta E, et al. MicroRNA-143 regulates adipocyte differentiation. *J Biol Chem*. 2004;279(50):52361–52365. doi:10.1074/jbc.C400438200
48. Li X, Zhao Y, Li X, et al. MicroRNA-150 modulates adipogenic differentiation of adipose-derived stem cells by targeting notch3. *Stem Cells Int*. 2019;2019:2743047. doi:10.1155/2019/2743047
49. Li X, Peng B, Zhu X, et al. MiR-210-3p inhibits osteogenic differentiation and promotes adipogenic differentiation correlated with Wnt signaling in ERα-deficient rBMSCs. *J Cell Physiol*. 2019;234(12):23475–23484. doi:10.1002/jcp.28916
50. Hamam D, Ali D, Vishnubalaji R, et al. microRNA-320/RUNX2 axis regulates adipocytic differentiation of human mesenchymal (skeletal) stem cells. *Cell Death Dis*. 2014;5(10):e1499. doi:10.1038/cddis.2014.462
51. Ling H, Wen G, Feng S, et al. MicroRNA-375 promotes 3T3-L1 adipocyte differentiation through modulation of extracellular signal-regulated kinase signalling. *Clin Exp Pharmacol Physiol*. 2011;38(4):239–246. doi:10.1111/j.1440-1681.2011.05493.x
52. Sanchez V, Golyardi F, Mayaki D, et al. Negative regulation of angiogenesis by novel micro RNAs. *Pharmacol Res*. 2019;139:173–181. doi:10.1016/j.phrs.2018.11.010
53. Li J, Diao S, Yang H, Cao Y, Du J, Yang D. IGFBP5 promotes angiogenic and neurogenic differentiation potential of dental pulp stem cells. *Dev Growth Differ*. 2019;61(9):457–465. doi:10.1111/dgd.12632
54. Zou T, Dissanayaka WL, Jiang S, et al. Semaphorin 4D enhances angiogenic potential and suppresses osteo-/odontogenic differentiation of human dental pulp stem cells. *J Endod*. 2017;43(2):297–305. doi:10.1016/j.joen.2016.10.019
55. Lee SI, Kim SY, Park KR, Kim EC. Baicalein promotes angiogenesis and odontoblastic differentiation via the BMP and Wnt pathways in human dental pulp cells. *Am J Chin Med*. 2016;44(7):1457–1472. doi:10.1142/S0192415X16500816
56. Basak S, Sarkar A, Mathapati S, Duttaroy AK. Cellular growth and tube formation of HTR8/SVneo trophoblast: effects of exogenously added fatty acid-binding protein-4 and its inhibitor. *Mol Cell Biochem*. 2018;437(1–2):55–64. doi:10.1007/s11010-017-3095-9
57. Kurtovic S, Ng TT, Gupta A, et al. Leptin enhances endothelial cell differentiation and angiogenesis in murine embryonic stem cells. *Microvasc Res*. 2015;97:65–74. doi:10.1016/j.mvr.2014.09.004
58. Arderiu G, Peña E, Aledo R, et al. MicroRNA-145 regulates the differentiation of adipose stem cells toward microvascular endothelial cells and promotes angiogenesis. *Circ Res*. 2019;125(1):74–89. doi:10.1161/CIRCRESAHA.118.314290
59. Li Q, Zhao H, Chen W, Huang P, Bi J. Human keratinocyte-derived microvesicle miRNA-21 promotes skin wound healing in diabetic rats through facilitating fibroblast function and angiogenesis. *Int J Biochem Cell Biol*. 2019;114:105570. doi:10.1016/j.biocel.2019.105570
60. Shi XF, Wang H, Xiao FJ, et al. MiRNA-486 regulates angiogenic activity and survival of mesenchymal stem cells under hypoxia through modulating Akt signal. *Biochem Biophys Res Commun*. 2016;470(3):670–677. doi:10.1016/j.bbrc.2016.01.084

61. Zhang J, Li S, Li L, et al. Exosome and exosomal microRNA: trafficking, sorting, and function. *Genomics Proteomics Bioinformatics*. 2015;13(1):17–24. doi:10.1016/j.gpb.2015.02.001
62. Bartel DP. MicroRNAs: genomics, biogenesis, mechanism, and function. *Cell*. 2004;116(2):281–297. doi:10.1016/S0092-8674(04)00045-5
63. Anderson J, McNally A. Biocompatibility of implants: lymphocyte/macrophage interactions. *Semin Immunopathol*. 2011;33(3):221–233. doi:10.1007/s00281-011-0244-1
64. Biermann AC, Marzi J, Brauchle E, et al. Impact of T-cell-mediated immune response on xenogeneic heart valve transplantation: short-term success and mid-term failure. *Eur J Cardiothorac Surg*. 2018;53(4):784–792. doi:10.1093/ejcts/ezx396
65. Pigott JH, Ishihara A, Wellman ML, Russell DS, Bertone AL. Investigation of the immune response to autologous, allogeneic, and xenogeneic mesenchymal stem cells after intra-articular injection in horses. *Vet Immunol Immunopathol*. 2013;156(1–2):99–106. doi:10.1016/j.vetimm.2013.09.003
66. Pelizzo G, Avanzini MA, Icaro Cornaglia A, et al. Extracellular vesicles derived from mesenchymal cells: perspective treatment for cutaneous wound healing in pediatrics. *Regen Med*. 2018;13(4):385–394. doi:10.2217/rme-2018-0001
67. Zhang W, Bai X, Zhao B, et al. Cell-free therapy based on adipose tissue stem cell-derived exosomes promotes wound healing via the PI3K/Akt signaling pathway. *Exp Cell Res*. 2018;370(2):333–342. doi:10.1016/j.yexcr.2018.06.035